

Adversarially-Trained Deep Nets Transfer Better

Francisco Utrera*

Department of EECS
University of California, Berkeley
utreraf@berkeley.edu

Evan Kravitz*

Department of EECS
University of California, Berkeley
kravitz@berkeley.edu

N. Benjamin Erichson

ICSI and Department of Statistics
University of California, Berkeley
erichson@berkeley.edu

Rajiv Khanna

Department of Statistics
University of California, Berkeley
rajivak@berkeley.edu

Michael W. Mahoney

ICSI and Department of Statistics
University of California, Berkeley
mmahoney@stat.berkeley.edu

Abstract

Transfer learning has emerged as a powerful methodology for adapting pre-trained deep neural networks to new domains. This process consists of taking a neural network pre-trained on a large feature-rich source dataset, freezing the early layers that encode essential generic image properties, and then fine-tuning the last few layers in order to capture specific information related to the target situation. This approach is particularly useful when only limited or weakly labelled data are available for the new task. In this work, we demonstrate that adversarially-trained models transfer better across new domains than naturally-trained models, even though it's known that these models do not generalize as well as naturally-trained models on the source domain. We show that this behavior results from a bias, introduced by the adversarial training, that pushes the learned inner layers to more natural image representations, which in turn enables better transfer.

1 Introduction

While deep neural networks (DNNs) achieve state-of-the-art performance in many fields, they are known to be “data hogs” that require large quantities of reasonably high-quality labelled data, which can often be expensive to obtain. As such, transfer learning has emerged as a powerful methodology that can significantly ease this burden by enabling the user to adapt a pre-trained DNN to a range of new situations and domains [3, 30]. In particular, models that are pre-trained on ImageNet have stunning transfer learning capabilities after fine-tuning only a few of the last layers [19] on the target domain.

Transfer learning was originally motivated by the observation that humans apply previously learned knowledge to solve new problems with ease [4]. With this motivation, the goal of transfer learning is to extract knowledge from one or more source tasks and apply the knowledge to a target task [23]. The obvious benefits include a reduction in the number of required labelled data points in the target domain [12, 23], and a reduction in training costs as compared to training a model from scratch. However, in practice, transfer learning remains an “art” that requires an experienced user who knows how to tune the many knobs of the transfer process. An important consideration, for example, is which concepts or features are transferable from the source domain to the target domain. The features which are specific to the individual domain cannot be transferred, and so an important goal of transfer learning is to hunt for features across domains.

In another line of work, it has recently been shown that adversarially-trained models (henceforth denoted as robust models) capture more *robust* features, that are more aligned with human perception, compared to the (to humans, at least) seemingly patternless features of standard models [14]. Unfortunately, these models typically have a *lower* generalization performance on the source domain, as compared to the naturally-trained model. Hence, Ilyas et al. [14] hypothesize that *non-robust* features that are lost during adversarial training may have a significant positive impact on generalization *within* a given dataset or domain. This inherently different feature representation between models constructed with adversarial training and models trained with standard methods would also explain why accuracy and robustness are at odds [28]. Naturally, this leads to the question of whether models that use robust representations generalize better *across* domains than those which only use non-robust features. This is the main question we address.

*Equal contributions.

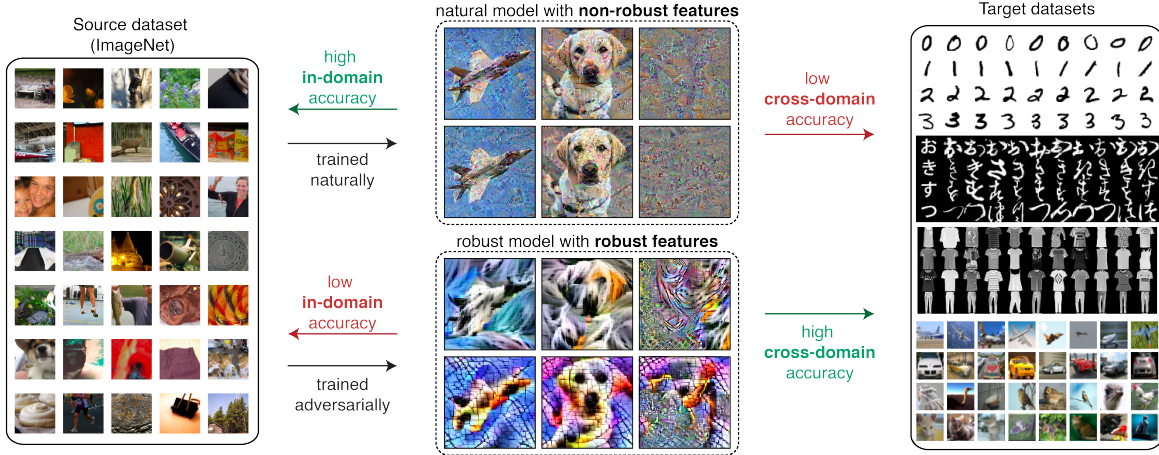


Figure 1: We demonstrate that adversarially-trained (i.e. robust) source models generalize better across domains. This agrees with the fact that robust models are equipped with *robust* features that encode representations that are more humanly perceptible, such as textures, strokes and lines. The introduced bias is so strong that even when random Gaussian noise is used as the starting seed it’s transformed into a mosaic of patterns, as seen in the rightmost (third) column for the robust model. We can visualize robust features by maximizing the activations in the penultimate layer using out of distribution images (i.e., images that are not part of the training and test data) as our starting seeds, following the “feature visualization” technique as implemented in [9]. We use an adversarially-trained ResNet-50 on ImageNet after fine-tuning the last fully-connected layer on CIFAR-10.

In this work, we demonstrate that adversarially-trained models transfer better to new domains than naturally-trained models. To demonstrate this, we conduct an extensive number of transfer learning experiments across multiple domains (i.e., datasets), with various numbers of fine-tuned convolutional blocks and random subset sizes from the target dataset, where the key variable is the constraint used to adversarially train the source model. (This is described in detail in sections 3 and 4.) Importantly, note that we do not use an adversarial training procedure for the actual transfer learning process. Our findings clearly indicate that adversarially-trained models have outstanding transfer learning characteristics across all configurations, where we measure the performance in terms of model accuracy on target datasets for varying numbers of training images and epochs. Figure 1 provides a summary of our approach.

Our focus in this work is to show that adversarially-trained source models learn representations which transfer better to new datasets. This is because adversarial training effectively *denoises* the features and learns higher quality representations for images. It does so by retaining the robust features of images that are independent of the idiosyncrasies present in the particular training data, and thus these models exhibit better performance when transferred. This observation is novel, and we undertake extensive empirical studies to make the following contributions.

- We show that adversarially-trained source models on ImageNet consistently achieve higher accuracy on target datasets than naturally-trained networks, after fine-tuning.
- We show that adversarially-trained source models improve their *relative* performance, as compared to naturally-trained models, when they are fine-tuned with fewer number of training examples from the target dataset and/or over fewer training epochs.
- We show that there is a connection between the degree of similarity between the source and target domains and the choice of transfer learning parameters that maximize the accuracy on the target dataset, such as the number of fine-tuning blocks, and the magnitude of the adversarial constraint.
- We perform a qualitative study to interpret robust representations using influence functions, and we observe that adversarially-trained source models better capture the class-level semantic properties of the images, consistent with human concept learning and understanding.

2 Related Work

Broadly, techniques in transfer learning can be taxonomized into several categories, depending on the nature of the source and target data. This categorization of approaches in transfer learning helps us formally specify an answer to the following three critical questions when solving a transfer learning problem: “what” to transfer; “how” to transfer; and

“when” to transfer. “What to transfer” refers to the specific knowledge present in the source domain that would adequately benefit a learning algorithm in the target domain. “How to transfer” refers to the specific algorithms developed to perform the transferring. Finally, “when to transfer” formally defines when a source and target domain are sufficiently related such that transferring knowledge between them is beneficial. Although important, the last question is a largely unexplored question in literature.

ImageNet transfers . Our focus is studying the transfer of all but the last few layers of trained DNNs and fine-tuning the last non-transferred layers. For ease of exposition, we restrict our attention to ImageNet models [8]. Kornblith et al. [19] study the transfer of naturally-trained models to various datasets, and is thus a prequel to our work. Yosinski et al. [30] also study transferring naturally-trained models but focus on the importance of individual neurons on transfer learning. They study the effect of depth within the network and optimization issues with regards to splitting networks between co-adapted neurons. Recht et al. [24] study the generalization of naturally and adversarially-trained models to additional data generated using a process similar to that of generating ImageNet. They conclude that models trained on ImageNet overfit the data. However, they study generalization of the model as-is without any fine-tuning applied to the last layers.

Covariate shift. A significant challenge in transfer learning is how to handle the change in distribution of the data across different domains, also called covariate shift. It has been widely recognized in successful domain adaptations [30, 11] that the representations in earlier (i.e., lower) layers are more “generic” and hence more transferable than the ones in later layers. This hierarchical disentanglement is attributed to the properties of the data itself, so that the later layers are more closely associated with the data and do not transfer as well. This has motivated studies for shallow transfer learning [30, 10] and more general studies to extract invariant features that remain invariant across different data distributions [1]. Further, several works attempt to mitigate the effect of domain shifts by mapping the feature sets into a common space, for example by minimizing some measure of the shift using a metric such as maximum mean discrepancy [29, 20], or a correlation metric [27, 26].

Robustness to adversarial attacks. Perhaps the closest work to ours is that by Shafahi et al. [25]. Their main motivation is somewhat different because they look into the following question: “How robust to PGD attacks are pre-trained adversarial models after fine-tuning to a new target dataset?” They find that models tend to lose more robustness as more layers are fine-tuned on the target dataset. More importantly, they find that a adversarially pre-trained model with a $\|\delta\|_\infty \leq 5$ constraint on ImageNet has lower accuracy on the target datasets, CIFAR-10 and CIFAR-100, compared to a naturally pre-trained ImageNet model. This might seem to contradict our thesis. However, the ϵ they used to adversarially train the source model is higher than the values we used in the two models that transfer “better.” In addition, as we explain later in section 5, adversarially-trained models on ImageNet with a high ϵ tend to underperform ones that use smaller ϵ , when fine-tuning to CIFAR-10 and CIFAR-100 (see Figure 5(c)).

Example based interpretability. There has been significant interest in interpreting blackbox models using salient examples from the data. A line of research focuses on using influence functions [17, 18, 15] to choose the most indicative data points for a given prediction. In particular, [15] discusses the connection of influence functions with Fisher kernels; and [16] proposes using criticisms in addition to representative examples. Complimentary lines of research focus on interpretability based on human understandable concepts (e.g., see [2]) and feature saliency metrics (e.g., see [21] and references within).

3 Explaining the Adversarial Training Process.

Adversarial training modifies the objective of minimizing the average loss across all data points by first maximizing the loss produced by each image with a perturbation (i.e., a mask) that may not exceed a specified magnitude. Here, we describe this process in more detail.

Let (\mathbf{x}_i, y_i) be m data points for $i \in [m]$, where $\mathbf{x}_i \in \mathbb{R}^d$ is the i^{th} feature vector, and $y_i \in \mathcal{Y}$ is the corresponding response value. Typically, we model the response as a parametric model $h_\theta : \mathbb{R}^d \rightarrow \mathcal{Y}$ with a corresponding loss function $\ell : \mathcal{Y} \times \mathcal{Y} \rightarrow \mathbb{R}_{\geq 0}$. The objective is to minimize the loss $\ell(\hat{y}, y)$, where $\hat{y} = h_\theta(\mathbf{x})$ is the predicted response. To make the model resilient to arbitrary perturbations of inputs, the above minimization problem of training the model is replaced by a minimax optimization problem of adversarial training. The goal of *adversarial training* is to solve a problem of the form

$$\min_{\theta} \frac{1}{m} \sum_{i=1}^m \max_{\|\delta_i\|_p \leq \epsilon} \ell(h_\theta(x_i + \delta_i), y_i). \quad (1)$$

That is, the goal is to find the parameters θ of the model h_θ that minimize the average maximum loss obtained by perturbing every input x_i with a δ_i constrained such that its ℓ_p norm does not exceed some non-negative ϵ . If $\epsilon = 0$, then $\delta_i = \mathbf{0}$, in which case there is no perturbation to the input, which is what we call *natural training*. As ϵ increases, the magnitude of the perturbation also increases. In practice, we solve (1) using stochastic gradient descent (SGD) over θ . More concretely, we include a random sample of training examples in a set B , specify a non-negative learning rate α , calculate the gradient with respect to the parameters of the model ∇_θ , and update θ as follows:

$$\theta := \theta - \frac{\alpha}{|B|} \sum_{(x_i, y_i) \in B} \nabla_\theta \max_{\|\delta_i\|_p \leq \epsilon} \ell(h_{\theta_i}(x_i + \delta_i), y_i). \quad (2)$$

This training process has a sequential nature: it first finds the worst possible perturbation δ_i^* for each training example (x_i, y_i) in B before updating the parameters of the model θ , where

$$\delta_i^* = \operatorname{argmax}_{\|\delta_i\|_p \leq \epsilon} \ell(h_\theta(x_i + \delta_i), y_i). \quad (3)$$

Problem (3) is typically solved using projected gradient descent with k update steps, which is what we call PGD(k). In this work, we use PGD(20), which means that we take 20 update steps to solve (3). Each step iteratively updates δ_i by projecting the update onto the ℓ_p ball of interest:

$$\delta_i := \mathcal{P}(\delta_i + \alpha \nabla_{\delta_i} \ell(h_\theta(x_i + \delta_i), y_i)). \quad (4)$$

As an example, consider the case of the ℓ_2 norm and let $f(\delta_i) = \ell(h_\theta(x_i + \delta_i), y_i)$. If we want to meet the restriction that $\|\delta_i\|_2 \leq \epsilon$, we can pick an update value for δ_i whose ℓ_2 norm will be at most the learning rate. This yields the problem:

$$\operatorname{argmax}_{\|v\|_2 \leq \alpha} v^\top \nabla_{\delta_i} f(\delta_i) = \epsilon \frac{\nabla_{\delta_i} f(\delta_i)}{\|\nabla_{\delta_i} f(\delta_i)\|_2}. \quad (5)$$

And in the case of the ℓ_∞ norm we have

$$\operatorname{argmax}_{\|v\|_\infty \leq \alpha} v^\top \nabla_{\delta_i} f(\delta_i) = \epsilon \cdot \operatorname{sign}(\nabla_{\delta_i} f(\delta_i))$$

Thus, we set the learning rate to be equal to $\alpha = c \cdot \frac{\epsilon}{\text{num. of steps}}$ for $1.5 < c < 4$ in order to ensure that we reach the boundary condition for δ_i . Also we must clip δ_i according to the ℓ_p norm in case that it exceeds the boundary condition.

4 Experimental Setup

We designed a comprehensive and fully reproducible study that considers an extensive set of transfer learning configurations. Every source model uses the exact same transfer learning variables: the number of unfrozen convolutional blocks, target datasets, and random subsets. This allows us to make a fair comparison between the naturally-trained ImageNet source model, as our control group, versus the adversarially-trained ImageNet source models, as our experimental group. We run each trial with several different seed values and report the mean and 95% confidence interval given the inherent variability in choosing random subsets of the target dataset for fine-tuning.

Source models. For all of our experiments, we use 4 residual networks (ResNet-50) [13] that were pre-trained on the ImageNet dataset [8], one was naturally-trained (without an adversarial constraint), and the others use PGD(20) and the following adversarial constraints: (1) $\|\delta\|_2 \leq 2$, (2) $\|\delta\|_\infty \leq \frac{4}{255}$, (3) $\|\delta\|_\infty \leq \frac{8}{255}$, where δ is a matrix that contains represents the perturbation applied to the input image as described in Section 3, equation (1). In addition to the naturally-trained ResNet-50, considered as baseline, we also use three adversarially-trained networks with various constraints. For speed, transparency and reproducibility, we do not re-train the source models ourselves.²

Fine-tuning procedure. To transfer our models we copy the entire source model to the target model, freeze the all but the last k convolutional blocks, re-initialize the last fully-connected (FC) layer for the appropriate number of classes, and *only* fine-tune (re-train) the last FC layer plus 0, 1, 3, or 9 convolutional blocks. Freezing layers in the neural networks entails permitting forward propagation, but disabling the back-propagation of gradients used during SGD training. The block freezing experimental setup we have developed yields a total of 4 different fine-tuning configurations, one for each number of fine-tuned convolutional blocks. Note that the ResNet model that we consider has residual blocks that are composed of three convolutional layers, i.e., we fine-tune 27 layers plus the fully connected layer when the number of fine-tuned blocks is equal to 9. (See Section B in the supplementary material for more a visualization of our fine-tuning process).

²The models that we use are provided as part of by the following repository: <https://github.com/MadryLab/robustness>.

Target datasets. We transfer our models to a broad set of target datasets, including (1) CIFAR-100, (2) CIFAR-10, (3) SVHN, (4) FMNIST, (5) KMNIST and (6) MNIST. Since all of these datasets have images at a lower resolution than ImageNet, we up-scale our images with bi-linear interpolation. In addition, we use common data transform techniques such as random cropping and rotation that are well-known to produce high-quality results with certain datasets.

Random subsets. One of the most interesting parts of our experimental setup is that we also explore the test accuracy of our fine-tuned models using randomly chosen subsets of 100, 200, 400, ..., and 25,600 images from the target dataset. These subsets are constructed using random sampling without replacement, with a minor constraint: all classes must have at least one training image. For each run of model training, we fix the training data to be a randomized subset of the entire training data. As the number of images in a random subset decreases, the variance in the validation accuracy of the transferred models increases. Thus, we repeat the fine-tuning procedure using 20 seeds for every subset with at most 1,600 images, and using 10 seeds for all larger subsets. We reduce the number of seeds for larger subsets because the inherently lower variance in the validation accuracy doesn't justify paying the computational cost associated to fine-tuning more seeds.

Altogether, we have a comprehensive and replicable experimental setup that considers 4 ImageNet source models, 4 fine-tuning configurations, 6 target datasets, 10 random subset sizes, and an average of 15 random seeds for a grand total of 14,400 fine-tuned models ($4 \times 4 \times 6 \times 10 \times 15$).

5 Results and Discussion

In this section, we present results that support our thesis that models with robust representations (i.e., adversarially-trained models) generalize better *across* domains than those which also use non-robust features (i.e., naturally-trained models). Furthermore, we show that adversarially-trained models have an even *larger* relative advantage over natural ones, when labelled data and/or computation are scarce resources, i.e., when models are fine-tuned using fewer labelled images from the target dataset and/or over fewer training epochs. Finally, we further investigate the effects of the number of fine-tuned blocks and adversarial constraints on test accuracy in detail and the impact of the similarity of between the source and target datasets. Our code is available at https://github.com/utrerf/robust_transfer_learning.git.

Adversarially-trained deep nets transfer better. In this section we pick the adversarially-trained (i.e., robust) model that transfers with the highest test accuracy across all datasets, which uses an $\|\delta\|_2 \leq 3$ constraint. Additionally, we fine-tune 3 convolutional blocks because it allows both the natural and robust models to achieve the highest accuracy on the target datasets.

The relative performance of the robust model is higher than the naturally-trained model regardless of the number of images used from the target dataset, as shown in Figure 2. Subplot 2(a) displays the test accuracy on each of the target datasets for various subset sizes, while Subplot 2(b) shows the test accuracy delta between the robust and natural models.

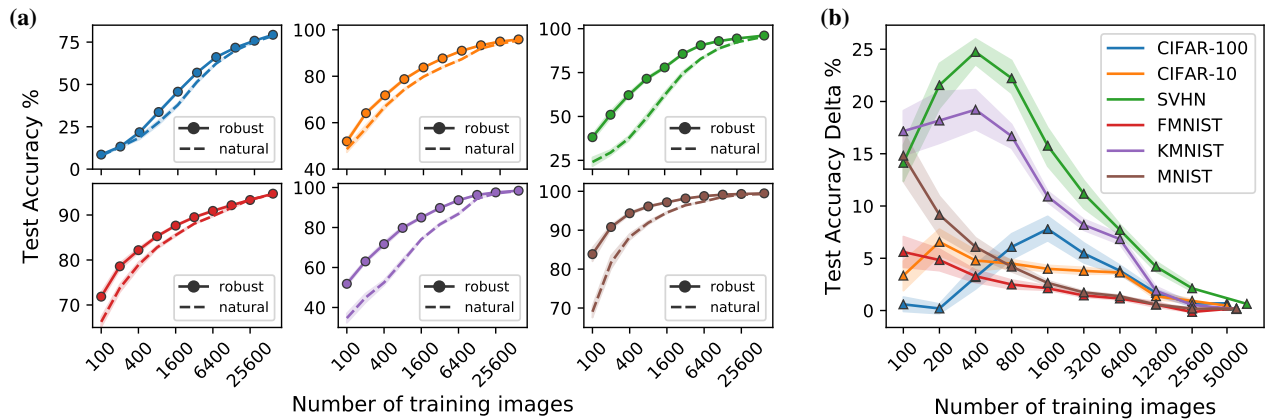


Figure 2: Robust models transfer better, in particular when fewer training images from the target domain are available. Robust model was adversarially-trained on ImageNet with an $\|\delta\|_2 \leq 3$ constraint. Both models fine-tune 3 convolutional blocks. (a) Test accuracy on each of the 6 target datasets (color-coded as in (b)) for various subset sizes. (b) Test accuracy delta defined as the robust model test accuracy minus natural model test accuracy. Solid line is the mean and its shade is the 95% confidence interval.

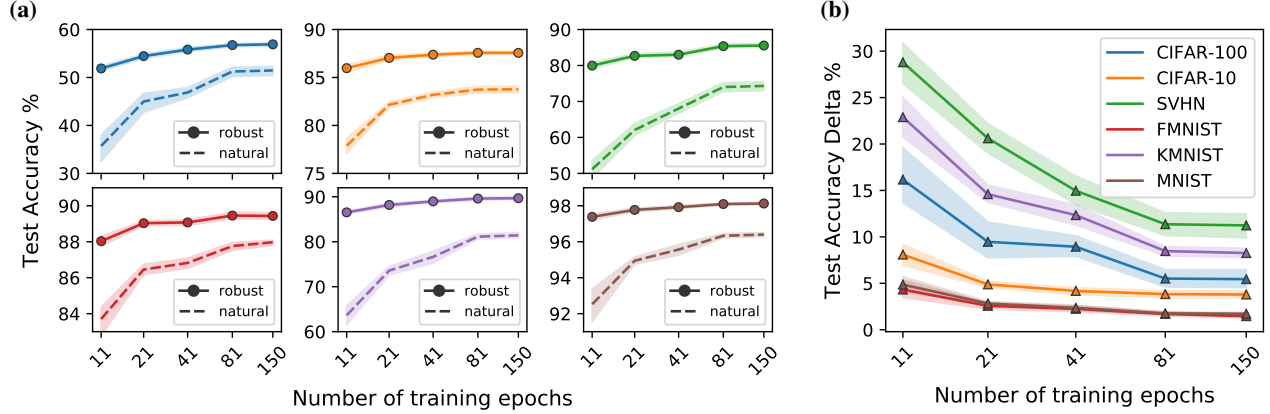


Figure 3: Robust models transfer faster. Robust model was adversarially-trained on ImageNet with a $\|\delta\|_2 \leq 3$ constraint. Both models fine-tune 3 convolutional blocks using a random subset of 3,200 images ($\sim 5\%$) of the target dataset. (a) Test accuracy during the fine-tuning process on each of the 6 target datasets (color-coded as in (b)) over training epochs. (b) Test accuracy delta defined as the robust model test accuracy minus the natural model test accuracy. Solid line is the mean and its shade is the 95% confidence interval.

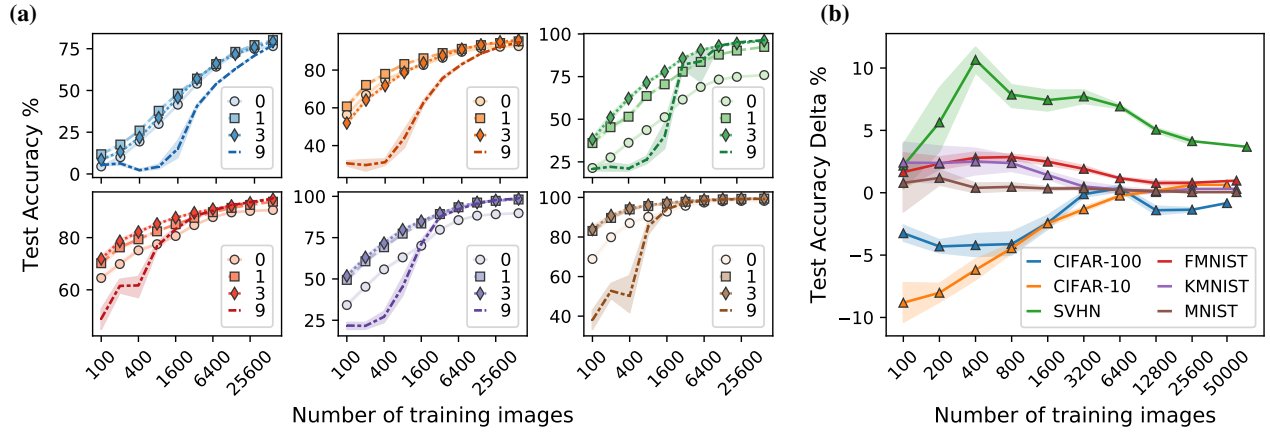


Figure 4: Effect of varying the number of convolutional blocks to fine-tune (the optimum is usually somewhere between 1 and 3). (a, b) Test accuracy of a robust model trained on ImageNet with a $\|\delta\|_2 \leq 3$ constraint with various number of fine-tuned blocks (0, 1, 3, or 9). (a) Test accuracy on each of the 6 target datasets (color-coded as in (b)). (b) Test accuracy delta between fine-tuned blocks, defined as 3 minus 1 fine-tuned blocks accuracy. Solid line is the mean and its shade is the 95% confidence interval.

In particular, when the test accuracy delta is above zero, the robust model outperforms the natural model. We see that the accuracy delta is above zero across all subset sizes and all datasets, which provides strong evidence to support that adversarially-trained models deep neural nets transfer better.

Adversarially-trained models also learn faster, as shown by Figure 3. In this figure, we use the models transferred with 3,200 images, which is approximately 5% of the target datasets. Subplot 3(a) displays the test accuracy on each of the target datasets for training epochs, while Subplot 3(b) shows the test accuracy delta: robust model minus natural test model accuracy. We can see that the robust model learns significantly faster, as evidenced by the large test accuracy delta in the first 11 and 21 epochs and the quickly flattening learning curve for the robust model.

Optimal configurations. Adversarially-trained models achieve the highest test accuracy on the target datasets when the right number of convolutional blocks are fine-tuned and when these models are trained with an appropriate constraint type and ϵ magnitude. In particular, we find that (1) fine-tuning 1 to 3 blocks works best, and (2) training with an ℓ_2 norm works better than an ℓ_∞ norm.

Fine-tuning too few or too many convolutional blocks leads to lower test accuracy on the target datasets, as shown in Figure 4(a). Each plot shows the test accuracy on the target datasets for the robust model that uses an ℓ_2 constraint with an

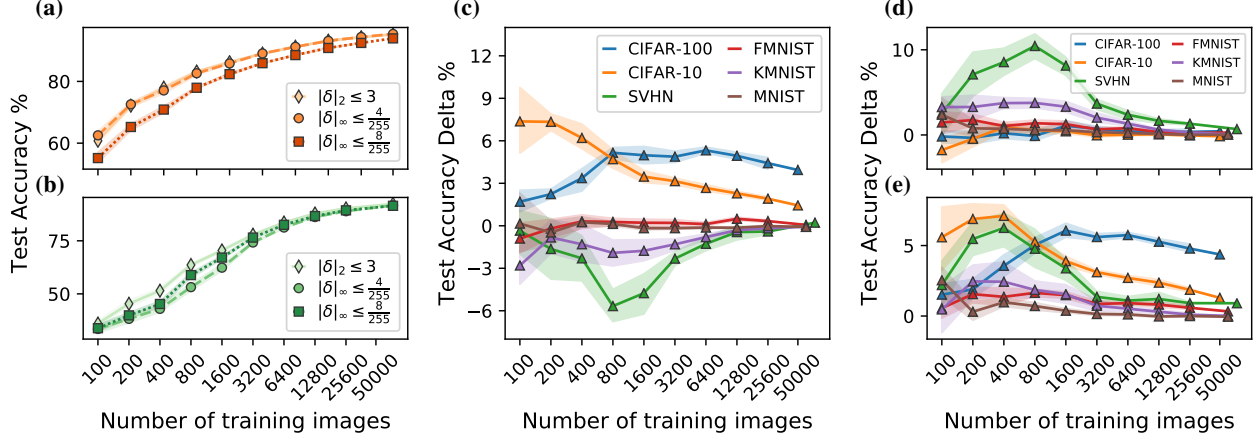


Figure 5: Test accuracy on target datasets, (a) CIFAR-10 and (b) SVHN, of 3 robust models pre-trained with various constraints on ImageNet. (c) Lower ϵ magnitudes perform better in target domains similar to the source domain, as shown by the test accuracy delta between the $\|\delta\|_\infty \leq \frac{4}{255}$ and the $\|\delta\|_\infty \leq \frac{8}{255}$ model. (d, e) Test accuracy delta between the ℓ_2 norm with $\epsilon = 3$ and each of the two ℓ_∞ models: $\epsilon = \frac{4}{255}$ in (d), and $\epsilon = \frac{8}{255}$ in (e). In both (d, e) the ℓ_2 norm constraint outperforms both of the ℓ_∞ constraints.

ϵ of 3. The same plot for the natural model and the two other adversarially-trained models are included in Section E of the supplementary material. They exhibit the same behavior across source models: fine-tuning 0 (only the fully-connected layer) or 9 convolutional blocks leads to lower test accuracy than fine-tuning 1 or 3 blocks.

Figure 4(b) helps us better understand how to pick a number of fine-tuned blocks, between 1 and 3. We define the test accuracy delta as: 3 blocks minus 1 block fine-tuned model accuracy. Consistent with the discussion in the “Similarity effect” subsection (below), the exact number of fine-tuned blocks seems to be a function of the level of similarity between the source and target datasets, with an increasing importance as the number of training images from the target dataset decreases.

Next, we want to analyze what is the best constraint type and ϵ . To do so, we consider the results of fine-tuning 3 convolutional blocks in 3 robust source models. We focus on 3 fine-tuned blocks since it allows the robust models to achieve the highest test accuracy on the target dataset, as discussed in Figure 4. Figure 5(a, b) display the test accuracy on the target datasets, CIFAR-10 (a) and SVHN (b).

A smaller ϵ performs better than a larger ϵ when fine-tuning to target datasets similar to the source dataset, as shown in Figure 5(c). We define test accuracy delta as: $\epsilon = \frac{4}{255}$ minus $\epsilon = \frac{8}{255}$ model accuracy. Hence, a positive test accuracy delta implies that a the model that uses a lower ϵ outperforms the one with a higher ϵ . See the the “Similarity effect” subsection for more details.

The robust model trained with an ℓ_2 constraint outperforms both models trained with an ℓ_∞ constraint, as shown in Figures 5(d, e). Test accuracy delta is defined as ℓ_2 norm with $\epsilon = 3$ minus each of the ℓ_∞ models: $\epsilon = \frac{4}{255}$ in (d), and $\epsilon = \frac{8}{255}$ in (e). We see that the ℓ_2 norm outperforms the ℓ_∞ norm. In particular, we see a statistically significant positive accuracy delta in (d) and (e) for some target datasets, as shown by the lower bound of the shaded region being above zero.

Similarity effect. Besides noticing that adversarially-trained models achieved better performance on the target dataset than naturally-trained models, we also observed trends in how different datasets transfer. When transferring from ImageNet, we found that CIFAR-10 and CIFAR-100 have interesting transfer properties, compared to the other datasets. In particular, even though all other datasets transfer better when fine-tuning 1 to 3 blocks, it seems that CIFAR-10 and CIFAR-100 do better when we fine-tune fewer blocks, which is shown in Figure 4. This suggests that because these datasets are close to ImageNet, fine-tuning of additional early blocks is unnecessary. Along similar lines, it is better to use a smaller ϵ for CIFAR-10 and CIFAR-100 datasets than the other datasets when transferring from ImageNet, as seen from Figure 5. This is because a larger perturbation would destroy the useful low-level features in ImageNet which are needed to classify CIFAR-10 and CIFAR-100 datasets. Finally, for datasets that are the most distinct from ImageNet (SVHN and KMNIST), we find that robustness adds the greatest benefit to classification accuracy and learning speed, as seen in Figure 2 and Figure 3 respectively. These discrepancies are the even more noticeable when only a fraction of the total number of training images are used.

6 Interpreting Representations using Influence Functions

In this section, we use the concept of influence functions [5, 6] to address the question of whether robust representations hold semantic information, e.g., suggesting that adversarially-trained DNNs classify images like a human would, through similar-looking examples. To do so, recall that Engstrom et. al. [9] observed that adversarially-learned representations exhibit properties such as invertibility and latent space arithmetic, so that moving the image in carefully chosen directions in the latent space allows for high level human-understandable feature manipulation in the pixel space. They suggest that the bias introduced by adversarial training can be viewed as a *human prior* on the representations, so that these representations are extractors of high-level human-interpretable features. Here, we study whether these representations aid the neural network *learn* new concepts (namely image classes) akin to how humans learn concepts. It has long been established that humans learn new concepts through concept-representative or similar-looking examples [7, 22].

To study this, we make use of influence functions [17] (see the supplementary material for an overview). For each of the train and test images of CIFAR-10, we use influence functions to ask “What is the influence of each training image on the model prediction for each training or testing image?” for both the naturally and robustly transferred (with $\|\delta\|_2 \leq 3$) models with 3 fine-tuned blocks and 3,200 labelled CIFAR-10 images. See Figure 6, which shows a randomly selected representative example for each of the 10 categories in the test set. For example, given the test image of a orange truck (on the far right) the top influential training image for the robust model is a similar-looking orange truck, the natural model has a blue and white truck. Overall, we noticed that for the robust model, the most influential images are often perceptibly similar to the respective test images, as opposed to the natural model. We observe a similar representational behavior to that shown in Figure 6 throughout CIFAR-10.

Figure 7 shows the influence values (standardized by their matrix norm) of each training image on each training (a and b) or testing (c and d) image index, sorted by their class, for both the natural and robust setups. (The order of the blocks

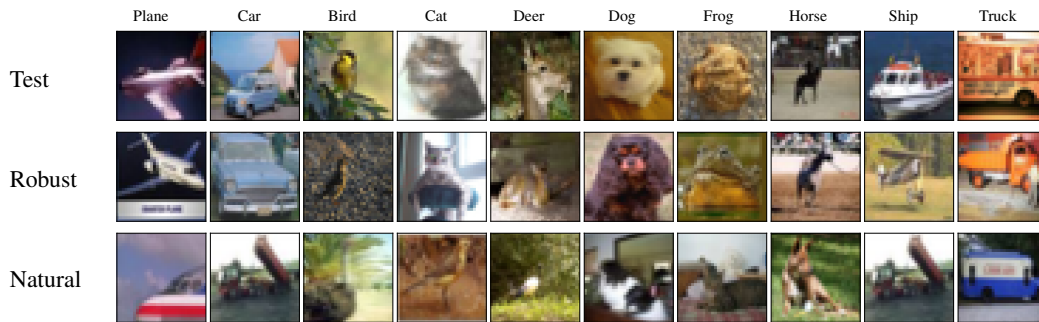


Figure 6: Adversarially-trained source models have more intuitive influential images in the target dataset. The top row contains the test image, one from each of the 10 categories. The remaining rows contain the most influential images in training set, for the pre-trained robust and pre-trained natural models, respectively.

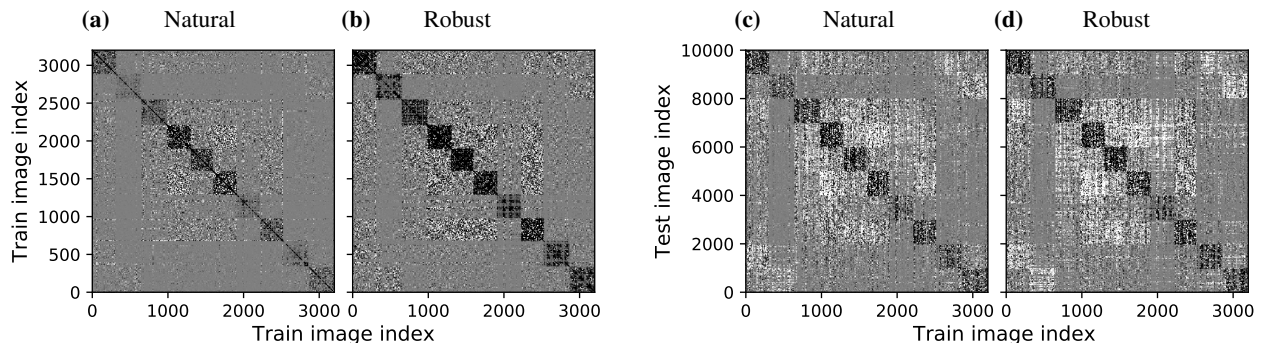


Figure 7: We present influence values for train/test images in this figure. Darker color represents a higher normalized influence value. The x-axis represents the influential image index for each train (a and b) or test (c and d) image index in the y-axis. Both axes are grouped by their true class. More defined and darker blocks on the diagonal for robust models indicate that influence values are more consistent with the correct underlying class for the robust model as compared to the natural model.

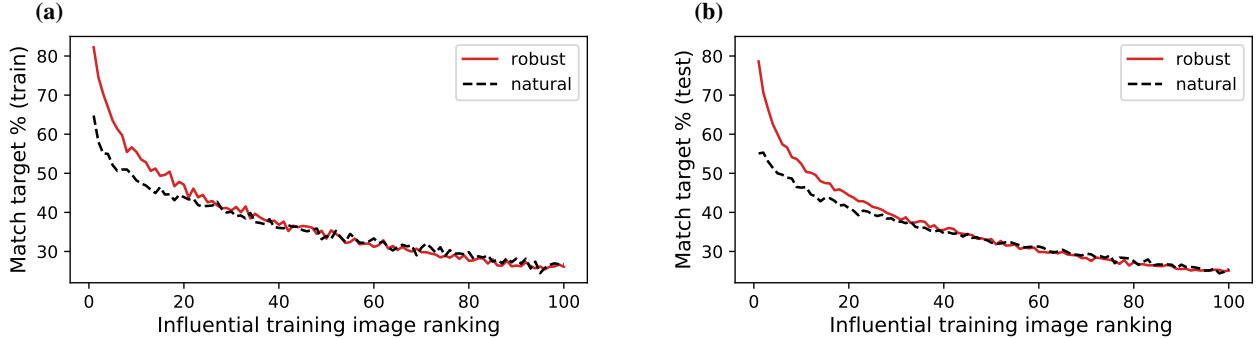


Figure 8: The classes of the top influential images for adversarially-trained source models match the classes of the target images more often than the naturally-trained ones. (a) shows the proportion of top-1 through top-100 influential images that match the target using training images, while (b) does the same but using testing images as targets.

corresponds to the classes in the order of the images in Figure 6.) In Figure 7, a darker color represents a higher influence value, gray corresponds to near-zero influence, and white represents a negative influence value. In particular, darker and better-defined blocks across the main diagonal signal that the influence values are more consistent with the class of the image index in the y-axis (test or train).

Since nominal influence value can arguably be incomparable across the natural and robust model (even after standardization), we also look at the percentage of top influential images that share the same class in Figure 8. Figure 8(a) is concerned with training images, while Figure 8(b) is concerned with testing images. To understand better this figure, take the leftmost point in the chart for both models. This represents the number of top-1 influential images in the training set that match the label of the given test or train image, in (a) or (b) respectively. Thus, the top influential image matches the test image category in 78.6% of cases for the robust models, as compared to 55.1% for the natural model, as seen in (b). We also consider the case when the category of at least 3 of the top-5 influential training images matches with that of the test image. This happens in 77.3% cases for the robust model, but only for 53.79% cases for the normal model. This vast gap is not explainable solely from only $\sim 5\%$ difference in accuracy (from Table 3 in the supplement). Thus, the robust model has learnt representations with more human-identifiable semantic information than the natural model, while the latter relies on less interpretable and more purely data-driven curve fitting. In context of the classification task, the robust neural network has *learnt* about the image classes in a more similar way to example-based concept learning in human beings, grouping similar examples closer (in the Fisher space [15]) in its internal representations. This reinforces the *human prior* bias in robust representations observed by Engstrom et. al. [9].

7 Conclusion

We have shown that adversarially-trained models transfer very well *across* domains, even outperforming naturally-trained models. This may be surprising, since they do not generalize as well *within* the source domain as naturally-trained models, and since they were originally designed to protect against adversarial attacks. In particular, we show that DNNs can be transferred both faster and with higher accuracy, while also requiring fewer images to achieve suitable performance on the target domain. We also show that the improved classification accuracy is due to the fact that robust models have an implicit bias that enables them to comprehend human-aligned features. Given the widespread use of DNNs, there is great potential for adversarially-trained networks to be applied to a variety of high-tech areas such as facial recognition, self-driving cars, and healthcare, but understanding the issues we have addressed is crucial to deliver upon that potential.

Acknowledgments. We are grateful for the generous support from Amazon AWS and Google Cloud. N.B. Erichson and M. W. Mahoney would like to acknowledge ARO, IARPA, NSF, and ONR as well as the UC Berkeley CLTC for providing partial support of this work. Our conclusions do not necessarily reflect the position or the policy of our sponsors, and no official endorsement should be inferred.

References

- [1] Martin Arjovsky, Léon Bottou, Ishaan Gulrajani, and David Lopez-Paz. Invariant risk minimization. *CoRR*, abs/1907.02893, 2019.
- [2] David Bau, Bolei Zhou, Aditya Khosla, Aude Oliva, and Antonio Torralba. Network dissection: Quantifying interpretability of deep visual representations. In *Computer Vision and Pattern Recognition (CVPR)*, 2017.
- [3] Yoshua Bengio. Deep learning of representations for unsupervised and transfer learning. In *International Conference of Machine learning (ICML)*, 2012.
- [4] Rich Caruana. Learning many related tasks at the same time with backpropagation. In *Neural Information Processing Systems (NeurIPS)*. 1995.
- [5] S. Chatterjee and A.S. Hadi. *Sensitivity Analysis in Linear Regression*. John Wiley & Sons, New York, 1988.
- [6] S. Chatterjee, A.S. Hadi, and B. Price. *Regression Analysis by Example*. John Wiley & Sons, New York, 2000.
- [7] Marvin S. Cohen, Jared T. Freeman, and Steve Wolf. Metarecognition in time-stressed decision making: recognizing, critiquing, and correcting. 1996.
- [8] Jia Deng, Wei Dong, Richard Socher, Li-Jia Li, Kai Li, and Li Fei-Fei. Imagenet: a large-scale hierarchical image database. In *Computer Vision and Pattern Recognition (CVPR)*, 2009.
- [9] Logan Engstrom, Andrew Ilyas, Shibani Santurkar, Dimitris Tsipras, Brandon Tran, and Aleksander Madry. Adversarial robustness as a prior for learned representations, 2019.
- [10] Muhammad Ghifary, W. Bastiaan Kleijn, and Mengjie Zhang. Domain adaptive neural networks for object recognition. In *Pacific Rim International Conferences on Artificial Intelligence (PRICAI)*, 2014.
- [11] Xavier Glorot, Antoine Bordes, and Yoshua Bengio. Domain adaptation for large-scale sentiment classification: A deep learning approach. In *International Conference on Machine Learning (ICML)*, 2011.
- [12] Boqing Gong, Yuan Shi, Fei Sha, and Kristen Grauman. Geodesic flow kernel for unsupervised domain adaptation. In *Computer Vision and Pattern Recognition (CVPR)*, 2012.
- [13] Kaiming He, Xiangyu Zhang, Shaoqing Ren, and Jian Sun. Deep residual learning for image recognition. In *Computer Vision and Pattern Recognition (CVPR)*, 2016.
- [14] Andrew Ilyas, Shibani Santurkar, Dimitris Tsipras, Logan Engstrom, Brandon Tran, and Aleksander Madry. Adversarial examples are not bugs, they are features. In *Neural Information Processing Systems (NeurIPS)*, 2019.
- [15] Rajiv Khanna, Been Kim, Joydeep Ghosh, and Oluwasanmi Koyejo. Interpreting black box predictions using fisher kernels. In *Artificial Intelligence and Statistics (AISTATS)*, 2019.
- [16] Been Kim, Rajiv Khanna, and Oluwasanmi Koyejo. Examples are not enough, learn to criticize! criticism for interpretability. In *Neural Information Processing Systems (NeurIPS)*, 2016.
- [17] Pang Wei Koh and Percy Liang. Understanding black-box predictions via influence functions. In *International Conference on Machine Learning (ICML)*, 2017.
- [18] Pang Wei W Koh, Kai-Siang Ang, Hubert Teo, and Percy S Liang. On the accuracy of influence functions for measuring group effects. In *Neural Information Processing Systems (NeurIPS)*. 2019.
- [19] Simon Kornblith, Jonathon Shlens, and Quoc V. Le. Do better imagenet models transfer better? In *Computer Vision and Pattern Recognition (CVPR)*, 2019.
- [20] M. Long, Y. Cao, Z. Cao, J. Wang, and M. I. Jordan. Transferable representation learning with deep adaptation networks. *Transactions on Pattern Analysis and Machine Intelligence (TPAMI)*, 2019.
- [21] A. C. Öztireli M. Gross M. Ancona, E. Ceolini. A unified view of gradient-based attribution methods for deep neural networks. In *Neural Information Processing Systems (NeurIPS) workshops*, 2017.
- [22] Allen Newell. *Human problem solving*. Prentice-Hall, USA, 1972.

- [23] Sinno Jialin Pan and Qiang Yang. A survey on transfer learning. *Transactions on knowledge and data engineering (TPAMI)*, 2009.
- [24] Benjamin Recht, Rebecca Roelofs, Ludwig Schmidt, and Vaishaal Shankar. Do ImageNet classifiers generalize to ImageNet? In *International Conference on Machine Learning (ICML)*, 2019.
- [25] Ali Shafahi, Parsa Saadatpanah, Chen Zhu, Amin Ghiasi, Christoph Studer, David Jacobs, and Tom Goldstein. Adversarially robust transfer learning. In *International Conference on Learning Representations (ICLR)*, 2020.
- [26] Baochen Sun and Kate Saenko. Deep coral: Correlation alignment for deep domain adaptation. In *European Conference on Computer Vision (ECCV)*, 2016.
- [27] Baochen Sun, Jiashi Feng, and Kate Saenko. Return of frustratingly easy domain adaptation. In *AAAI Conference on Artificial Intelligence*, 2016.
- [28] Dimitris Tsipras, Shibani Santurkar, Logan Engstrom, Alexander Turner, and Aleksander Madry. Robustness may be at odds with accuracy. In *International Conference on Learning Representations (ICLR)*, 2019.
- [29] Eric Tzeng, Judy Hoffman, Ning Zhang, Kate Saenko, and Trevor Darrell. Deep domain confusion: Maximizing for domain invariance. *ArXiv*, abs/1412.3474, 2014.
- [30] Jason Yosinski, Jeff Clune, Yoshua Bengio, and Hod Lipson. How transferable are features in deep neural networks? In *Neural Information Processing Systems (NeurIPS)*, 2014.

A Additional Details on Influence Functions

Suppose that $\ell : \mathbb{R}^m \times \mathbb{R}^d \rightarrow \mathbb{R}$ is a smooth loss function and $x^1, \dots, x^n \in \mathbb{R}^m$ are our given data. The empirical risk minimization (ERM) problem takes the form

$$\min_{\theta \in \mathbb{R}^d} f(\theta) = \frac{1}{n} \sum_{j=1}^n \ell(x^j, \theta). \quad (6)$$

Say θ^* is the argmin solution of the above optimization problem. Let’s now consider upweighing a data point x_{train} with $\epsilon \in \mathbb{R}$. This modifies the learning problem as:

$$\min_{\theta \in \mathbb{R}^d} \frac{1}{n} \sum_{j=1}^n \ell(x^j, \theta) + \epsilon \ell(x_{\text{train}}, \theta). \quad (7)$$

Let θ_ϵ^* be the solution of the upweighted problem above. The *influence* of a training data point x_{train} on a test data point x_{test} approximates the change in the function value $\ell(x_{\text{test}}, \theta^*) \rightarrow \ell(x_{\text{test}}, \theta_\epsilon^*)$ with respect to an infinitesimally small ϵ , i.e., when $\epsilon \rightarrow 0$ when x_{train} is upweighed by ϵ . This can be calculated in closed form [17] as:

$$-g_1 H^{-1} g_2, \quad (8)$$

where $g_1 = \nabla \ell(x_{\text{train}}, \theta^*)^\top$, $g_2 = \nabla \ell(x_{\text{test}}, \theta^*)$ and H is the Hessian of the loss function $\nabla^2 f(\theta^*)$. In particular, we first compute the Hessian of the source model fine-tuned with 3,200 CIFAR-10 images as the sum of the Hessians of the loss of batches of 5 images. Note that we only use the 3,200 images that were used in the fine-tuning process, since it accurately reflects the Hessian of the model. Then we get H^{-1} using the (Moore-Penrose) pseudo-inverse, using its singular-value decomposition and including all singular values larger than $1e-20$.

Koh et. al. [17] discuss optimization speedup techniques to determine the most influential x_{train} for a given x_{test} at scale. However, finding top- k influential images is a combinatorial problem for $k > 1$. So, typically a greedy selection of the next top influential image is made iteratively k times. Further, selecting multiple images also requires consideration of interaction and group effects. As such, the top-5 influential images are likely to be less representative of actual influence being asserted than one would expect.

Fisher Kernels and Influence Functions Khanna et. al. [15] recently discovered an interesting relationship between Fisher Kernels and Influence functions: if the loss function $\ell(\cdot)$ can be written as a negative log-likelihood, then at the optimum w^* , the Fisher dot product between two points is exactly the same as the influence of those points on each other (note that the influence is a symmetric function). In other words, finding the most influential data point to a given data point is equivalent to finding the nearest neighbor of the point in the space induced by the Fisher kernel. As observed in Section 6 for robust training, most influential points for a data point tend to be largely the ones belonging to the same class. This implies that in the Fisher space, the points with the same class tend to be grouped together.

B Fine-Tuning Details

Figure 9 illustrates all 4 fine-tuning configurations in our experiments. Notice how in Subfigure 9(d) we unfreeze more than half of the ResNet-50 architecture, thereby testing what occurs as we fine-tune a lot of blocks.

All source models are fine-tuned to all datasets using stochastic gradient descent with momentum using the hyperparameters described in Table 1.

Table 1: Hyper-parameter summary for all fine-tuned source models

Learning rate	Batch size	Momentum	Weight decay	LR decay	LR decay schedule	Fine-tuned adversarially?
0.1	128	0.9	5×10^{-4}	10x	1/3, 2/3 epochs	No

The learning rate decays to a tenth of it’s current value every 33 or 50 epochs, which corresponds to 1/3 of the total fine-tuning epochs, as shown in Table 2. Also, the test accuracy frequency refers to how often is the test accuracy computed, in epochs. So, for example, if the test accuracy frequency is 20, then we check the test accuracy after epoch 1, 21, 41, ..., 81, and 100.

Table 2: Batch summary for every target dataset and source model

Number of images	Fine-tuning epochs	Number of random seeds	Test accuracy frequency (epochs)	LR decay schedule
100	100	20	20	33/66
200	100	20	20	33/66
400	100	20	20	33/66
800	100	20	20	33/66
1,600	100	20	20	33/66
3,200	150	10	10	50/100
6,400	150	10	10	50/100
12,800	150	5	10	50/100
25,600	150	5	10	50/100
All	150	1	10	50/100

With regards to the random seeds, we have the following formula to define the set of seeds used, S_k , as a function of the total number of random seeds used, k :

$$S_k = \{20000000 + (100000i) | i \in \{0, 1, \dots, k - 1\}\}. \quad (9)$$

Thus, when we use 20 seeds, as it is the case for the subset of 100 images, we use seeds 20000000, 20100000, ..., 21900000. Large numbers were used to avoid numerical instability issues that arise with small numbers where their binary representation has too many zeroes.

See Table 3 for additional detail with regards to the source models. Notice that although adversarially-trained models do worse on the source dataset, they outperform naturally-trained models on the target datasets, as shown in Table 5.

Table 3: Summary of source models trained on ImageNet, which we consider for transfer learning.

Pre-training Procedure	Constraint	ImageNet Test Accuracy
Natural	–	76.13%
Adversarial	$\ \delta\ _2 \leq 3$	57.90%
Adversarial	$\ \delta\ _\infty \leq 4/255$	62.42%
Adversarial	$\ \delta\ _\infty \leq 8/255$	47.91%

See Table 4 for a high-level overview of all datasets used. This should serve as a reminder that our source dataset is ImageNet, with an extensive 1.2 million training images and 1,000 classes, it serves as a great starting point in our experiments. All other target datasets have a considerably lower number of training and test images.

Table 4: Summary of the source and target datasets.

Dataset	Number of training images	Number of test images	Number of classes	Color or grayscale	Source or target
ImageNet	1.2 million	150,000	1,000	color	source
CIFAR-100	50,000	10,000	100	color	target
CIFAR-10	50,000	10,000	10	color	target
SVHN	73,257	26,032	10	color	target
FMNIST	60,000	10,000	10	grey-scale	target
KMNIST	60,000	10,000	10	grey-scale	target
MNIST	60,000	10,000	10	grey-scale	target

C Summary of Results

Table 5 reports the test accuracy of all of our source models after fine-tuning 3 blocks using different numbers of training images on each of the 6 target datasets. The average test accuracy is reported for all cases where the model is fine-tuned with less than the entire training set. The bolded numbers represent the highest test accuracy among source models. From this table, we can see that the robust models consistently outperform the natural models.

D Codebase Overview

Our code, available at https://github.com/utrerf/robust_transfer_learning.git, allows others to replicate the entire experiment. The starting point requires downloading the source ImageNet models, and installing the appropriate libraries. Next, the user can decide how to fine-tune the source models: individually or in batches. The `train.py` file will allow individual training, while the `tools/batch.py` file allows training in batches.

The `train.py` file contains 9 parameters that are explained by running the following command: `python train.py -help`. Also, the `helpers.py` and `delete_big_files.py` files under the `tools` folder contain the logic that supports the `train.py` file. This includes the random subset generator, the fine-tuning procedure, and the data transforms.

Separately, note that when running the `batch.py` file, the fine-tuned models won't be saved into the `results/logs` directory. This is due to the fact that models can occupy a significant amount of memory and we do not plan to use these fine-tuned models in the future. However, if the user wants to save the fine-tuned models, then he or she can do so by commenting our line 60 in the `batch.py` file: `deleteBigFilesFor1000experiment()`.

Lastly, all results are stored into the `results/logs` folder by default and can be compiled easily into a csv file using the `log_extractor.py` script.

E Additional Detail on the Effect of the Number of Fine-Tuned Blocks

The following subsection contains the additional charts that were omitted in Figure 4 in Section 5. Figure 10 shows the same behavior is observed in all 3 figures: It's sub-optimal to fine-tune either 0 or 9 convolutional blocks, as opposed to 1 or 3. Consistent with our methodology for Figure 4, we adversarially-train models on ImageNet and then fine-tune various numbers of convolutional blocks using a random sample of images in the target dataset.

Table 5: Summary of the test accuracy on target datasets after fine-tuning 3 blocks (9 convolutional layers). Reported average test accuracy for all cases where the model is fine-tuned with less than the entire training set.

Target dataset	Training images	Pre-training constraint on source dataset (ImageNet)			
		Natural	$\ \delta\ _2 \leq 3$	$\ \delta\ _\infty \leq \frac{4}{255}$	$\ \delta\ _\infty \leq \frac{8}{255}$
CIFAR-100	100	7.97	8.54	8.24	8.84
CIFAR-10	100	48.49	51.89	49.86	49.03
MNIST	100	23.5	37.9	34.75	35.75
FMNIST	100	66.11	71.8	71.24	72.69
KMNIST	100	34.29	51.76	50.12	51.05
MNIST	100	68.69	83.83	83.03	82.81
CIFAR-100	200	13.05	13.26	13.71	12.79
CIFAR-10	200	57.44	64.05	62.83	60.11
MNIST	200	29.37	50.89	46.82	47.77
FMNIST	200	73.53	78.51	77.67	78.33
KMNIST	200	44.77	62.97	60.36	62.84
MNIST	200	81.58	90.72	90.44	90.49
CIFAR-100	400	18.57	21.74	21.32	19.79
CIFAR-10	400	66.84	71.65	71.93	68.81
MNIST	400	37.3	61.97	58.99	61.02
FMNIST	400	78.8	82.09	81.4	81.58
KMNIST	400	52.45	71.65	70.18	71.89
MNIST	400	88.09	94.28	93.9	93.98
CIFAR-100	800	27.57	33.68	32.55	30.17
CIFAR-10	800	74.2	78.68	78.99	75.95
MNIST	800	49.17	71.19	68.84	70.19
FMNIST	800	82.73	85.21	84.6	84.59
KMNIST	800	63	79.67	77.73	80.68
MNIST	800	91.81	96.05	95.58	95.92
CIFAR-100	1,600	37.88	45.64	44.49	40.82
CIFAR-10	1,600	79.74	83.76	83.47	81.1
MNIST	1,600	62.14	77.84	75.24	76.77
FMNIST	1,600	85.39	87.58	87.09	86.91
KMNIST	1,600	74.06	84.95	83.66	85.52
MNIST	1,600	94.47	97.13	97	97.16
CIFAR-100	3,200	51.46	56.91	55.79	51.34
CIFAR-10	3,200	83.77	87.56	87.34	85.07
MNIST	3,200	74.31	85.55	81.57	84.4
FMNIST	3,200	87.97	89.43	89.11	88.89
KMNIST	3,200	81.42	89.68	88.26	89.14
MNIST	3,200	96.4	98.13	97.93	98.1
CIFAR-100	6,400	62.26	66.1	65.31	60.75
CIFAR-10	6,400	87.28	90.91	90.23	88.6
MNIST	6,400	82.63	90.46	88.17	89.09
FMNIST	6,400	89.63	90.73	90.44	90.11
KMNIST	6,400	86.7	93.61	91.7	92.86
MNIST	6,400	97.34	98.73	98.5	98.57
CIFAR-100	12,800	69.92	71.61	71.42	67.16
CIFAR-10	12,800	91.95	93.2	93.11	91.6
MNIST	12,800	88.7	92.86	91.68	91.81
FMNIST	12,800	91.56	92.09	91.97	91.69
KMNIST	12,800	94.32	96.21	95.73	95.9
MNIST	12,800	98.52	99.11	98.98	99.03
CIFAR-100	25,600	75.08	75.68	75.4	71.52
CIFAR-10	25,600	93.93	94.92	94.63	93.28
MNIST	25,600	92.24	94.36	93.76	93.91
FMNIST	25,600	93.42	93.24	93.14	92.79
KMNIST	25,600	97.01	97.52	97.34	97.44
MNIST	25,600	99.06	99.27	99.21	99.24
CIFAR-100	50,000	78.49	79.24	79.51	76.06
CIFAR-10	50,000	95.36	95.86	95.6	94.58
FMNIST	60,000	94.51	94.72	94.41	93.98
KMNIST	60,000	98.07	98.35	98.19	98.38
MNIST	60,000	99.19	99.42	99.34	99.39
MNIST	73,257	95.33	96.02	95.42	95.63

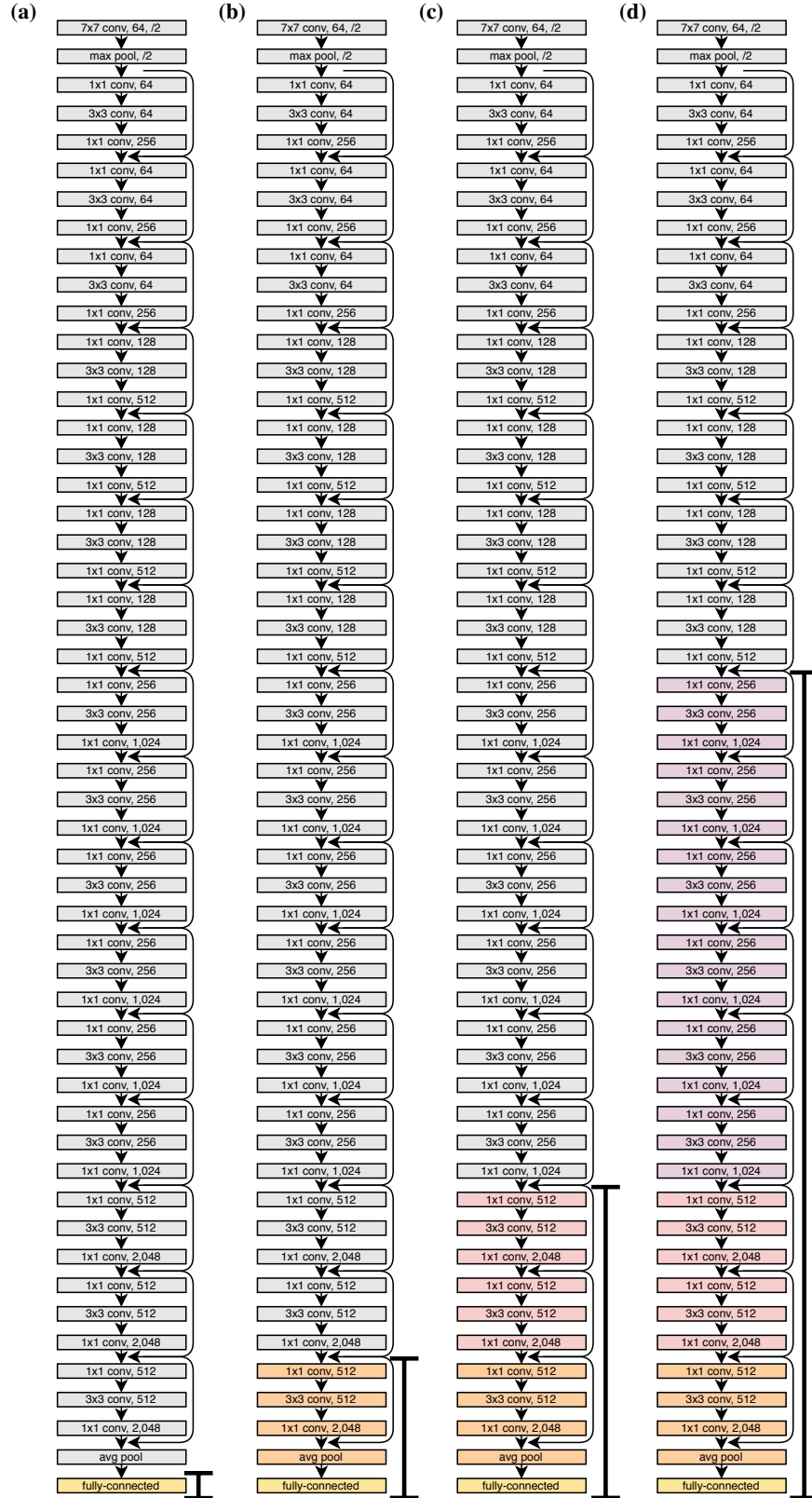


Figure 9: Fine-tuning setup: (a) 0 blocks. (b) 1 block. (c) 3 blocks (d) 9 blocks. Each block has 3 convolutional layers.

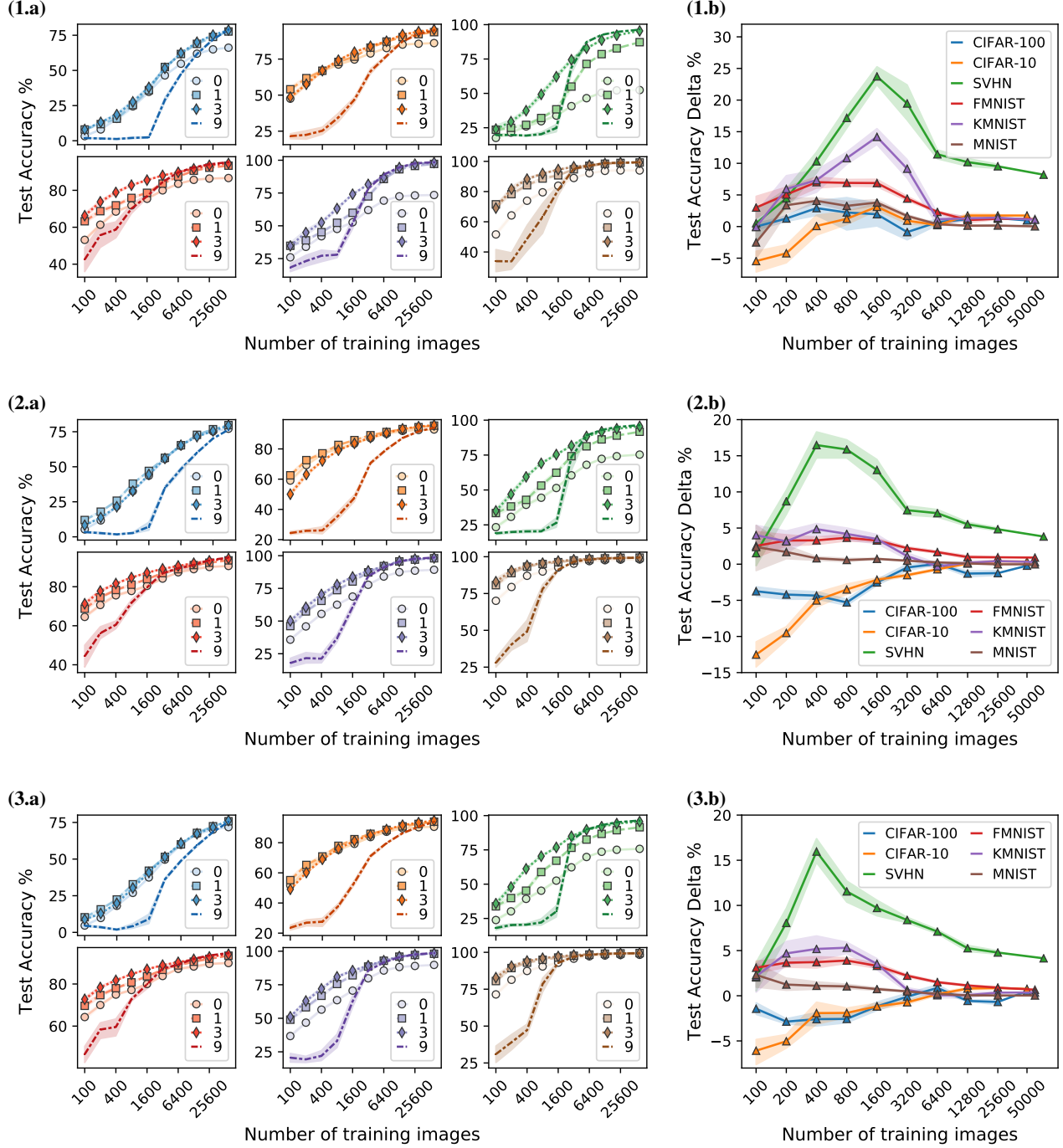


Figure 10: It's sub-optimal to fine-tune either 0 (only FC layer) or 9 convolutional blocks, as opposed to 1 or 3. (a) Test accuracy on each of the 6 target datasets (color-coded as in (b)) for various subset sizes and fine-tuning various number of blocks: 0, 1, 3, or 9. (b) Test accuracy delta defined as the test accuracy with 3 fine-tuned blocks minus the test accuracy with 1 fine-tuned block. Adversarial constraints used to train on the source dataset (ImageNet): (1) $\|\delta\|_2 \leq 3$, (2) $\|\delta\|_\infty \leq \frac{4}{255}$, or (3) $\|\delta\|_\infty \leq \frac{8}{255}$. The solid line is the mean and the shade is the 95% confidence interval.